



ATR-SEIRAS—an approach to probe the reactivity of Pd-modified quasi-single crystal gold film electrodes

S. Pronkin, Th. Wandlowski *

Institute for Thin Films and Interfaces ISG3, Research Centre Jülich, 52425 Jülich, Germany

Received 25 July 2003; accepted for publication 3 May 2004
Available online 29 July 2004

Abstract

Quasi-single crystalline gold films of 20 nm thickness and preferential (111) orientation on Si hemispheres were modified by controlled potentiostatic deposition of Pd (sub-ML, ML, multi-L) from sulphate and/or chloride-containing electrolyte. The electrochemical properties of these model electrodes were characterised for hydrogen and (hydrogen-) sulphate adsorption as well as for surface oxide formation by cyclic voltammetry. Conditions were developed to fabricate defined and stable Pd monolayers. In situ ATR-SEIRAS (Attenuated Total Reflection Surface Enhanced Infrared Reflection Absorption Spectroscopy) experiments were carried out to describe the electrochemical double layer of Pd modified gold film electrodes in contact with aqueous 0.1 M H₂SO₄ with focus on interfacial water and anion adsorption. Based on an analysis of the non-resonant IR background signal the potential of zero charge is estimated to 0.10–0.20 V (vs. RHE). CO was found to be weakly physisorbed in atop sites on Au(111-20 nm)/0.1 M H₂SO₄ only in CO saturated electrolyte. CO, deposited on a quasi-single crystal gold film modified with 1 ML Pd, is chemisorbed with preferential occupation of bridge sites and atop positions at step edges. Saturated CO adlayers, as obtained by deposition at 0.10 V, contain isolated water species and are covered by a second layer of hydrogen bonded water. Potentiodynamic SEIRAS experiments of CO electro-oxidation on Pd-modified gold film electrodes demonstrate clearly the existence of a “pre-oxidation” region. They also provide spectroscopic evidence that isolated water and weakly hydrogen bonded water are consumed during the reaction and that atop CO on defect sites is a preferential reactant. The simultaneous in situ monitoring of the potential- and time-dependent evolution of characteristic vibrational modes in the OH- and CO-stretching regions are in agreement with the Gilman (“reactant pair”) mechanism of CO oxidation.

© 2004 Elsevier B.V. All rights reserved.

Keywords: Infrared absorption spectroscopy; Carbon monoxide; Gold; Palladium; Metallic films; Electrochemical methods; Oxidation; Physical adsorption; Chemisorption; Surface defects; Vibrations of adsorbed molecules

* Corresponding author. Fax: +49 2461 61 3907.

E-mail address: th.wandlowski@fz-juelich.de (Th. Wandlowski).

URL: <http://www.fz-juelich.de/isg/isg3/tw/index.php>.

1. Introduction

The establishment of structure–reactivity relations at the atomic or molecular level is one of the major challenges of modern physical electrochemistry [1]. Fundamental aspects of reactivity in electrochemical systems can be approached through the controlled modification of well-defined single crystal electrode surfaces by foreign metal overlayers [2]. Such systems exhibit often electronic, structural, chemical and catalytic properties quite different from those of the underlying substrate or of the bulk deposited materials [3,4]. Of particular interest are pseudomorphic adlayers obtained by controlled deposition of metal adlayers on a noble metal substrate. Pd deposited on Pt(*hkl*) [5–14] or Au(*hkl*) [15–30] electrodes represent model systems for these studies. Pd adlayers were prepared by physical vapour deposition in UHV [5,13], electrochemical [6,8,11,12,14,28] and chemical [7,9,30] strategies. The electronic and geometrical properties of pseudomorphic adlayers can be tuned by choosing template substrates with different electronic structures and lattice constants. As a consequence, the (electrocatalytic) reactivity of the metal overlayers can be significantly modified [8,9,13,29,31,32].

In this contribution we report the first in situ surface enhanced infrared spectroscopy (SEIRAS) [33,34] study of well defined ultrathin Pd deposits on quasi single crystalline gold film electrodes employing an internal attenuated total reflection (ATR) configuration. Osawa et al. pioneered the application of ATR-SEIRAS to equilibrium and time-resolved studies at electrochemical interfaces [33,34]. This technique is based on a thin metal film or metal colloid, which is used as a working electrode; deposited onto a highly refractive prism, such as Si or Ge. The IR beam passes through the prism and is totally reflected at the metal/electrolyte interface [33–35]. This in situ spectroscopic approach provides direct access to chemical information on structure and dynamics of the electrode/electrolyte interface as well as on reactions taking place there. ATR-SEIRAS investigations at (electro-) catalytically active electrified solid/liquid interfaces were previously reported for rough Pt [36–38] and Pt/Fe alloy [39] deposits prepared by

electrochemical plating [36], sputtering [37,39] or chemical deposition techniques [38,40]. The success of these studies is limited by one problem, which still hampers the development of defined structure–reactivity relations: The morphology of the (electro-) catalytically active deposits is not controlled and often rather arbitrary.

As an alternative approach we propose in this paper the design of bimetallic electrodes, composed of quasi-single crystalline template electrodes, which are subsequently modified by controlled deposition of Pt-group metals (submonolayer, monolayer and/or multilayer regime). This strategy adapts the advantages of ATR-SEIRAS on coinage metal substrates [33,34] and opens novel opportunities for in situ spectroelectrochemical studies of structure and reactivity of Pt-group metals under steady state and time-resolved conditions due to the following reasons: (1) high and specific surface sensitivity with an enhancement of the IR-response of physisorbed and chemisorbed species up to ca. 100 times stronger than those in conventional IRAS, (2) dominant first layer (Helmholtz region) effect with a probing range of a few nanometers, (3) no limitations due to mass transport and potential perturbation, e.g. the time resolution of the experiment is only limited by the time constant of double layer charging (<50 μ s in the present configuration) [33,34,41], (4) application of (1)–(3) to the fabrication and study of well-defined (electro-) catalytic and SEIRAS-active Pt-group model electrodes, such as Pd, Rh and Pt, employing quasi-single crystalline coinage metal film templates.

The electrochemical preparation and characterisation of defined Pd-modified gold film electrodes benefits from the detailed knowledge on the initial stages of Pd deposition on massive Au(*hkl*) electrodes. The potentiostatic deposition of Pd on Au(*hkl*) was studied with electrochemical techniques, the quartz crystal microbalance (EQCM), in situ scanning tunnelling microscopy (STM), and surface X-ray scattering (SXS) [8,14–23,25–29]. Pd, the lattice constant of which is about 4.8% smaller than that of Au, grows epitaxially on the low index faces of Au, and forms rather flat overlayers [8,16–20,22,23,25]. The Pd deposition on Au(111) and Au(100) starts with a pseudomorphic layer in the underpotential regime, and

proceeds subsequently at overpotentials. STM measurements reveal up to four pseudomorphic monolayers for Pd on Au(111). The largest terrace size was found in 1 ML films, thicker deposits decrease the domain size and increase the surface roughness [19,22]. The modified Au(111) electrodes approach the electrochemical properties of massive Pd(111) for thicker deposits [8,15,26]. No Pd–Au surface alloy formation was found on Au(111) [19], but clear evidence was reported on Au(100) and Au(110) [20,25]. Recently, the adsorption of hydrogen/(hydrogen-) sulphate ions and oxide formation/reduction of thin Pd overlayers on Au(*hkl*) have been investigated employing cyclic voltammetry and electrochemical transient techniques [15,23,26]. Electrocatalytic properties were explored for the oxygen reduction [21], the oxidation of adsorbed CO [29], formic acid [8], formaldehyde [23] and methanol [42]. All studies demonstrate the unique electrochemical characteristics of the first Pd monolayer, a clear dependence of these reactions on Pd film thickness and substrate crystallography, and distinct differences to the properties of bulk Pd(*hkl*) [15,26,29,43,44].

The present article aims to characterize the electrochemical double layer and to explore the reactivity of Pd modified quasi single crystalline gold film electrodes employing simultaneously *in situ* ATR-SEIRAS and electrochemical techniques. The paper is organised as follows: experimental details are summarised in Section 2. The potentiostatic formation and electrochemical characterisation of Pd-modified gold film electrodes will be discussed next. Subsequently, *in situ* ATR-SEIRA spectroelectrochemical studies to describe the double layer properties of these model electrodes in sulphate containing aqueous electrolyte will be presented. Finally, we will demonstrate the potential of our novel approach for real time electrocatalytic studies, choosing the adsorption and oxidation of CO as test reactions.

2. Experimental

2.1. Quasi-single crystalline gold film electrodes

The quasi-single crystalline Au(111-20 nm) film electrodes were prepared by electron beam evapo-

ration (base pressure $< 2 \times 10^{-7}$ mbar, deposition rate 0.005–0.007 nm s⁻¹) of a 20 nm thick gold film onto the flat side of a silicon hemisphere (25 mm diameter). The metal coated silicon prism was either attached to an all-glass holder for carrying out electrochemical characterisation and deposition experiments in a hanging meniscus configuration in a three electrode cell (EC) or to a vertical spectroelectrochemical cell (IR-C) [41]. The geometrical area of the working electrode was either 4.9 cm² (EC) or 1.54 cm² (IR-C). The metal films were electrochemically annealed during deoxygenating of the electrolyte by cycling the potential in the double layer region with 10 or 50 mV s⁻¹ to generate well defined (111)-oriented terrace sites. In the following we will represent these electrodes by the abbreviation Au(111-20 nm).

2.2. Pd-deposition

The Pd adlayers were obtained by electrodeposition from (i) 0.1 M H₂SO₄ + 0.1 mM PdSO₄ at 0.75 V or (ii) 0.1 M H₂SO₄ + 0.1 mM PdCl₂ at 0.80 V vs. real hydrogen electrode (RHE, see below). The Au(111-20 nm) film electrode was brought in contact with the carefully deaerated Pd-containing electrolyte at open circuit (~ 1.05 V), and subsequently the potential was scanned with 50 mV s⁻¹ in the negative direction until the desired deposition potential was reached (for further details see Section 3.2). The latter value was kept constant, and simultaneously the corresponding charge flow was monitored. After the completion of the deposition, the modified electrode was carefully rinsed with Milli-Q water, and transferred into a Pd-free electrolyte for surface characterisation. Overlayers fabricated from Cl⁻-containing electrolyte were exposed to an additional conditioning step, which consists of polarisation at 0.10 V in 0.1 M H₂SO₄ to remove trace impurities of halide ions, and a subsequent solution exchange.

2.3. CO deposition

CO (4.7 N) was adsorbed on the bare or modified Au(111-20 nm) electrode surface at 0.10 V by injection of a mixture of Ar/CO into the electrolyte for 30 min to achieve saturation coverage.

Subsequently, the electrolyte was purged with Ar to remove CO from solution for additional 30 min.

2.4. Electrolyte solutions

The solutions were prepared with Milli-Q water (18 M Ω cm, estimated total organic content 2–3 ppb), H₂SO₄ (suprapure Merck), PdO (Aldrich, 99.999%) or PdCl₂ (Aldrich, 99.999%). All electrolytes were deaerated with argon (5 N) prior to and during each experiment. The measurements were carried out at 23 ± 1 °C. The glassware was cleaned in a 1:1 mixture of hot H₂SO₄ and HNO₃ followed by rinsing cycles with Milli-Q water.

2.5. Electrochemical measurements

The electrochemical measurements were carried out with an Autolab PGSTAT 30 in a three electrode configuration. The reference electrode was either a trapped hydrogen or a Hg/Hg₂SO₄/Na₂SO₄ sat. electrode. All potentials in this paper are quoted with respect to the real (trapped) hydrogen electrode (RHE: ~310 mV vs. SCE). The counter electrode was a large area platinum spiral.

2.6. SEIRAS set-up

The SEIRAS experiments were carried out in a vertical spectroelectrochemical cell. Details of the set-up were reported in a previous paper [41]. The IR-spectra were measured with a Bruker IF 66V/s Fourier Transform Spectrometer choosing a spectral resolution of 4 cm⁻¹. Unpolarised radiation from a global source was focused onto the electrode/electrolyte interface by passing through the modified Si-hemisphere. The incident angle was usually 70° referring to the surface normal. The IR radiation totally reflected at the interface was measured with a liquid nitrogen cooled detector (MCT 317, Colmar Technologies). Typically, 160 interferograms were scanned and co-added into each single beam spectrum during a slow potential scan. The spectra were plotted in absorbance units defined as $A = -\log(I/I_0)$, where I and I_0 represent the intensities of the reflected radiation

at the sample and the reference potentials, respectively. Positive going bands indicate accumulation of the species with respect to the reference spectrum.

3. Results and discussion

3.1. Characterisation of the bare quasi-single crystalline gold film electrodes

Fig. 1 shows typical i vs. E curves of an electrochemically annealed Au(111-20 nm) film electrode in 0.1 M H₂SO₄. The voltammograms exhibit well defined features of preferentially (111) oriented single crystalline electrodes, such as the lifting of the ($p \times \sqrt{3}$) reconstruction (P1) and the order/disorder phase transitions of a ($\sqrt{3} \times \sqrt{7}$) (hydrogen) sulphate overlayer (P2/P2'). Excursion into the oxidation region, at $E > 1.30$ V, shows a shoulder OA1 assigned to an oxidation process involving steps, and the characteristic peak OA2, which represents contributions from terrace sites [45,46]. Internal calibration experiments with massive stepped single crystals Au (nnn -2) revealed an equivalent miscut angle of 2–4°, which relates to an average size of ideally smooth terraces of 19–27 atoms [41]. Based on a comparison of the

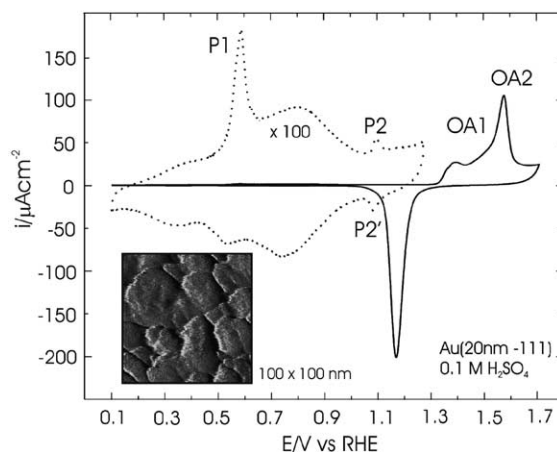


Fig. 1. Steady state cyclic voltammograms of a Au(111-20 nm) film electrode in contact with 0.1 M H₂SO₄, scan rate 10 mV s⁻¹, double layer (dotted line) and ox/red region (solid line). The inset shows a typical ex situ STM image of an electrode just after e-beam deposition of a 20 nm gold film on silicon.

charge balance in the oxidation/reduction region [46], for a chemisorbed uracil monolayer [47] as well as for Cu UPD [48] between carefully prepared Au(111-20 nm) film electrodes and well defined Au(*nnn*-2) stepped single crystals we estimated the electrochemically active area. The latter appears to be 1.6 times larger than the corresponding geometrical area.

3.2. Pd-covered quasi-single crystalline gold film electrodes—electrochemical deposition and characterisation

3.2.1. Deposition

The fabrication of Pd-modified Au(111-20 nm) film electrodes was carried out in the presence and in the absence of chloride-containing electrolyte. Fig. 2 shows typical current–potential curves for 0.1 mM PdCl₂ in 0.1 M H₂SO₄ recorded at 1 mV s⁻¹. The starting potential was chosen at 1.05 V, which is more positive than $E_{\text{pzc}} = 0.550$ V of the Au(111-20 nm) film electrode in contact with 0.1 M H₂SO₄ [41]. Under these conditions we may assume that the electrode surface is covered with adsorbed tetrachloropalladate (PdCl₄²⁻) ions [19]. During the negative and the subsequent positive potential scan one characteristic pair of cur-

rent peaks P1' = 0.885 V and P1 = 0.93 V is found in 0.85 V ≤ E ≤ 1.10 V. The charge consumed during a typical cathodic scan is estimated to 700 ± 70 μC cm⁻² and corresponds approximately to the formation (dissolution) of a pseudomorphic Pd monolayer involving two electrons per Au surface atom and considering the previously determined scaling factor of 1.6 (for further discussion see below and Fig. 4). Peak position and intensity do not change upon continuous cycling in this interval. Extending the potential window toward more negative values, e.g. E < 0.85 V, gives rise to an additional peak P2 on the positive potential scan. The latter increases with more negative return potentials and/or increasing waiting time at E < 0.85 V. The comparison of these observations with previously reported results for the Pd deposition on Au(111) massive single crystals [19] supports the following assignment: The pair of peaks P1/P1' represents the underpotential deposition (UPD) of a Pd monolayer on Au(111-20 nm) with preferential contributions from nucleation at defect (step) sites, and P2 corresponds to the dissolution of bulk deposited Pd. The equilibrium potential for Pd deposition from 0.1 M H₂SO₄ + 0.1 mM Pd²⁺ was determined to 0.82 V [49]. This value shifts more positive with higher concentration of Pd²⁺, and the deposition rate increases due to faster mass transport. Based on these experiments, we have chosen the following conditions for the modification of Au(111-20 nm) with Pd: sub-ML and ML Pd-coverages were obtained by immersing the electrochemically annealed electrode into deaerated electrolyte, 0.1 M H₂SO₄ + 0.1 mM PdCl₂ at 1.05 V, scanning the electrode potential with 50 mV s⁻¹ to a deposition potential in the UPD range, and waiting until the desired charge flow through the interface was consumed. Pd multilayers were fabricated by diffusion-controlled electrodeposition at E_d = 0.80 V. The inset of Fig. 2 shows a typical current vs. time transient representing the formation of approximately 1 ML Pd on Au(111-20 nm). Emersion of the electrode in the potential range 0.80 V ≤ E ≤ 0.90 V, careful rinsing, and subsequent transfer into a Pd²⁺-free solution results in a Au(111-20 nm) film modified irreversibly with Pd.

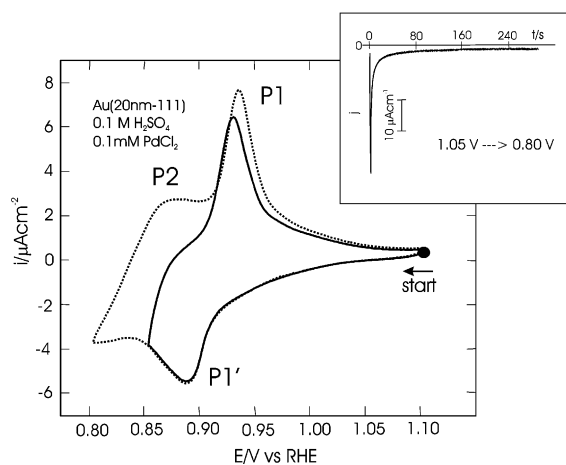


Fig. 2. Current vs. potential curves for Au(111-20 nm)/0.1 M H₂SO₄ + 0.1 mM PdCl₂, 1 mV s⁻¹ with negative return potentials of 0.85 V (solid line) or 0.80 V (dotted line). The inset shows a typical chronoamperometric transient for Pd deposition triggered by a fast potential scan from 1.05 V → 0.80 V (50 mV s⁻¹) and subsequent waiting at 0.80 V.

Similar experiments were also performed with 0.1 M $\text{H}_2\text{SO}_4 + 0.1 \text{ mM PdSO}_4$. The UPD of Pd is rather slow and starts approximately 50 mV more negative than in chloride-containing electrolyte. Repeated cycling in the UPD range yielded irreversible changes of the corresponding current vs. potential curves. In consequence, Pd-deposition on Au(111-20 nm) from chloride-free electrolyte was carried out at $E_d = 0.75 \text{ V}$, after immersion of the electrode at 1.05 V, and scanning the electrode potential with 50 mV s^{-1} to E_d .

3.2.2. Characterization

Typical voltammograms for Pd adlayers of 1 ML thickness (A, C) as well as for variable coverages (B, D) on Au(111-20 nm)/0.1 M H_2SO_4 , fabricated either in chloride-containing (A, B) or chloride-free (C, D) electrolyte, are presented in Fig. 3. Comparison with experiments on massive Au(111) [15,29] and Pd(111) [44,50] single crystals suggests a distinction between four different potential regions labelled I–IV in Fig. 3. The most neg-

ative region I, $E < 0.15 \text{ V}$, represents the hydrogen absorption, which occurs at higher overpotentials on Au(111-20 nm) as compared with massive Pd(111), and develops more pronounced with increasing film thickness (Fig. 3B and D). Region II, $0.15 \text{ V} \leq E \leq 0.40 \text{ V}$, is attributed to the coupled adsorption/desorption of hydrogen and (hydrogen-) sulphate [15]. Up to 1 ML equivalent of deposited Pd only one single pair of peaks with $E_{P2} = 0.30 \text{ V}$ (positive scan) and $E_{P2'} = 0.27 \text{ V}$ (negative scan) develops. The corresponding total charge is estimated to $Q_{\text{HA}} \approx 200 \pm 20 \mu\text{C cm}^{-2}$. With increasing Pd film thickness the peaks P2/P2' increase in magnitude, but remain asymmetrical. Starting from 2 ML Pd on Au(111-20 nm), a second anodic peak appears in region II at $E_{P3} \approx 0.27 \text{ V}$ (Fig. 3B and D). The corresponding cathodic peak was only resolved separately for Pd overlayers fabricated in Cl^- -containing electrolyte, $E_{P3'} = 0.265 \text{ V}$ (Fig. 3), but no other significant differences were found between the two deposition strategies. The observed hysteresis and the peak

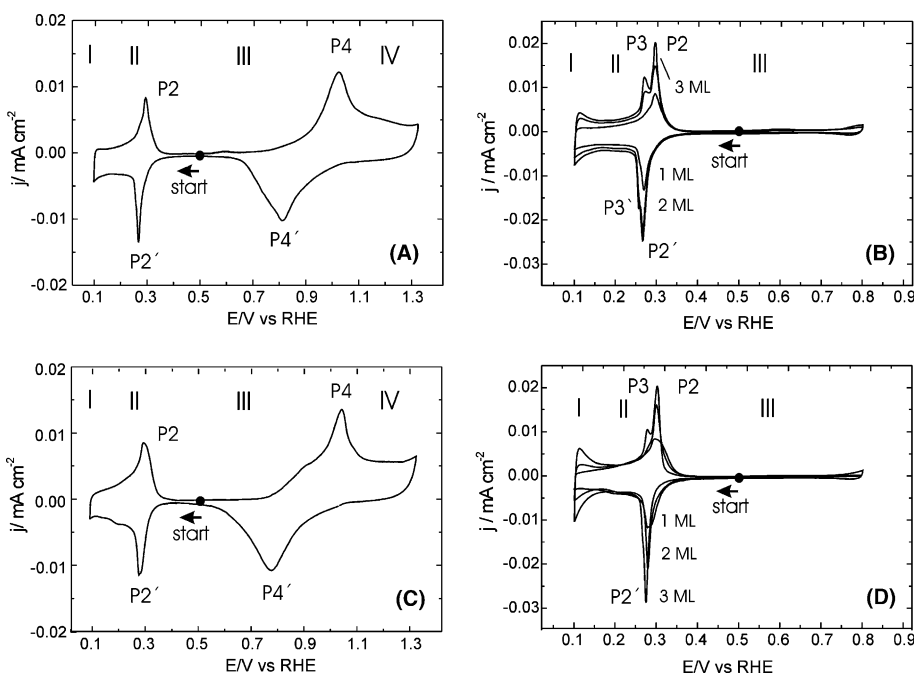


Fig. 3. Cyclic voltammograms for Pd deposited on Au(111-20 nm)/0.1 M H_2SO_4 from 0.1 mM PdCl_2 (A, B) or 0.1 mM PdSO_4 , 5 mV s^{-1} (C, D). The curves represent single potential scans after starting at 0.50 V, and scanning first in the negative direction. (A) and (C) represent 1 ML Pd, while (B) and (D) show current–potential curves of up to 3 ML Pd in two characteristic potential ranges. The stability ranges of the various adlayer/substrate phases are labelled I–IV.

shapes suggest the involvement of kinetically controlled adsorption/phase formation transitions. The systematic changes of the adsorption/desorption peaks for hydrogen and (hydrogen-) sulphate are accompanied, as demonstrated in studies with massive single crystals [15,19,26], by a gradual structural transition from a pseudomorphic Pd ML with lateral strain to thicker Pd films having bulk properties. Therefore, we attribute the two pairs of current peaks in region II to the presence of laterally strained (P2/P2') and bulk-like (P3/P3') Pd. In comparison to these rather broad peaks observed on Au(111-20 nm) and Au(111) [15], narrow adsorption spikes were reported for Pd(111) [26,44,50] and Pd–Pt(111) [5,7,14].

The potential interval III, which extends between 0.40 and 0.80 V, reveals a wide double layer charging region without faradic contributions, rather independent of the Pd coverage (we investigated up to 5 equivalent ML Pd). Electrochemical and in situ STM studies with Pd(111) and Pd–Au(111) [15,44,50] suggest that the modified film electrode is covered with specifically adsorbed (hydrogen-) sulphate. At this stage we also like to stress that extended potential cycling in 0.10 V ($I \leq E \leq 0.80$ V (III)) does not change the current potential profiles. This observation suggests that surface alloying of Au and Pd [51] is either rather slow or does not take place.

The potential region IV, at $E > 0.80$ V, is attributed to the surface oxidation of the Pd adlayers [26,44,50]. The single scan voltammograms as monitored during the first positive potential excursions for 1 ML Pd–Au(111-20 nm)/0.1 M H_2SO_4 (Fig. 3A and C) exhibit a characteristic oxidation peak P4 at $E_{P4} \approx 1.02$ V and a corresponding reduction feature P4' at $E_{P4'} \approx 0.75$ V. The position of P4 is approximately 0.10 V, respective 0.20 V more negative than for the same process on Pd(111) [29,50] or 1 ML Pd–Pt(111) [7], and its overall morphology compares reasonably with results reported for 1 ML Pd–Au(111)-3° miscut/0.1 M H_2SO_4 [29,44,50]. The potential for the reduction of 1 ML Pd oxide is just in-between the published values for Pd(111) (~ 0.70 V) [26,44,50] and an ideal pseudomorphic Pd ML on a perfect Au(111) single crystal (~ 0.81 V) [29]. The charge balance between oxidation and

reduction as well as repetitive potential cycling demonstrate that oxide formation causes irreversible changes, most probably related to Pd dissolution. Similar observations were also reported for Pd(111) [50] and pseudomorphic Pd ML adsorbed on an ideally smooth Au(111) surface [29].

3.2.3. Calibration “master curve”

The above analysis of Pd–Au(111-20 nm) film electrodes in 0.1 M H_2SO_4 reveals that the charge density due to (hydrogen-) sulphate desorption/hydrogen adsorption, Q_{HA} , and its anodic counterpart might be chosen as quantitative measures for the composition of the surface structure. Comparing the estimated values of Q_{HA} with the deposited amount of Pd on Au(111-20 nm) film electrodes, Q_{Pd} , results in a “calibration master curve” with two distinct slopes, 0.28 ± 0.03 and 0.028 ± 0.004 , respectively (Fig. 4). The intersection point was found at $Q_{Pd} = 0.72 \pm 0.08$ $mCcm^{-2}$ and $Q_{HA} = 0.20 \pm 0.02$ $mCcm^{-2}$. This plot includes data from experiments carried out in the electrochemical (hanging meniscus configuration: ■, ●) or the spectroelectrochemical cell (○) for Pd modification in the absence (●, ○) as well as in the presence (■) of chloride-containing electrolyte.

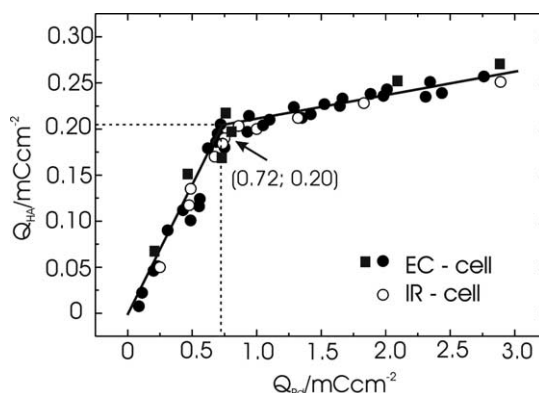


Fig. 4. Calibration master curve. The charge density consumed in the hydrogen adsorption/anion desorption region II (peaks P2'/P3'), Q_{HA} , is plotted vs. the charge density of Pd deposition, Q_{Pd} , for experiments carried out in an electrochemistry cell in hanging meniscus configuration (■, ●) or in the SEIRAS cell after subsequent steps of solution exchange (○) for depositions of Pd from 0.1 M H_2SO_4 + 0.1 mM $PdSO_4$ (●, ○) or 0.1 mM $PdCl_2$ (■).

The formation of a pseudomorphic Pd ML on an ideally smooth Au(111) surface consumes a charge of 0.444 mCcm^{-2} . Taking this reference and considering the “electrochemical roughness” of our Au(111-20 nm) templates of 1.6, we conclude that the charge $Q_{\text{Pd}} = 0.72 \text{ mCcm}^{-2}$ at the intersection point corresponds to approximately one equivalent ML of Pd. The charge Q_{HA} is slightly lower than the accordingly scaled value for 1 ML Pd–Au(111)/0.1 M H_2SO_4 [15], but agrees well with preliminary data of CO charge displacement experiments for hydrogen ($E = 0.10 \text{ V}$, $Q_+ = 0.15 \pm 0.02 \text{ mCcm}^{-2}$, cf. Fig. 9A) and anion adsorption ($E = 0.40 \text{ V}$, $Q_- = -0.06 \pm 0.02 \text{ mCcm}^{-2}$). The small difference to the charge balance of an ideal Au(111) surface might indicate that, under our experimental conditions, the consumption of one equivalent ML charge of Pd deposition does not completely cover the entire Au(111-20 nm) electrode. The emerging growth of a second Pd layer, even not yet detectable in the current potential profiles for $Q_{\text{Pd}} \approx 0.72 \pm 0.14 \text{ mCcm}^{-2}$ (Fig. 3), might take place at local spots.

Nevertheless, the above data and discussion demonstrate that we can establish in our experiments conditions to fabricate well-defined Pd monolayers on Au(111-20 nm) templates. These electrodes were employed in the in situ SEIRAS studies to explore double layer structure and reactivity in the absence and in the presence of CO as model reactant.

3.3. In situ SEIRA spectra of 1 ML Pd on quasi-single crystalline gold film electrodes

3.3.1. Overview

Fig. 5 shows a typical series of SEIRA spectra for 1 ML Pd–Au(111)/0.1 M H_2SO_4 (black lines) as measured in $0.10 \text{ V} \leq E \leq 0.80 \text{ V}$, e.g. within the double layer regions II and III (cf. Fig. 3), during a positive potential sweep with 10 mVs^{-1} . The grey lines represent the SEIRA spectra of the bare gold film before modification with Pd. A set of single beam spectra acquired at 0.17 V , e.g. within the potential region of hydrogen adsorption, was chosen as reference [15]. This potential is expected to be rather close to the potential of zero charge, E_{pzc} , of 1 ML Pd–Au(111-20 nm)/0.1 M H_2SO_4 .

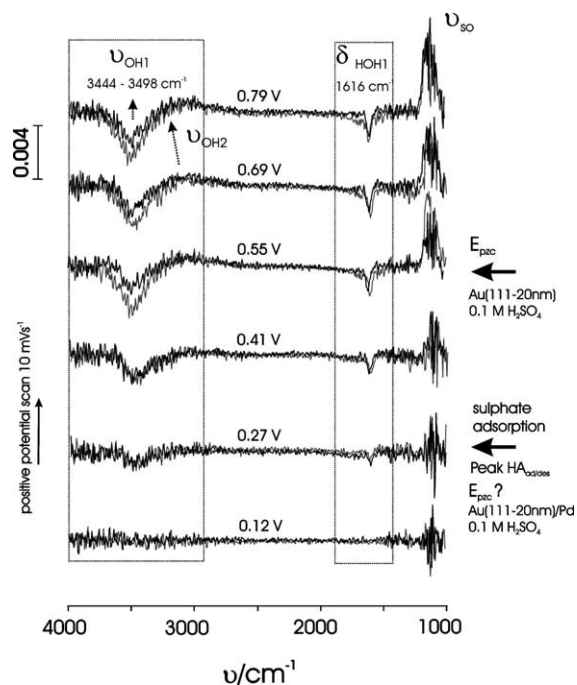


Fig. 5. Selected SEIRA spectra of Au(111-20 nm)/0.1 M H_2SO_4 (grey lines) + 1 ML Pd (black lines) as a function of potential. The spectra were acquired during a potential sweep with 10 mVs^{-1} between 0.10 and 0.80 V vs. RHE. The reference potential is 0.17 V. Every plotted spectrum represents the average of a potential interval of 50 mV.

The following observations motivate and support this hypothesis. (i) The potential of zero charge, E_{pzc} , of 1 ML Pd–Au(111) and of Pd(111) in the absence of specifically adsorbed ions have been determined as 0.23 and 0.20 V [28]. These values are 0.32 V respective 0.35 V more negative than E_{pzc} of an ideal Au(111)-(1 × 1) electrode in contact with 0.01 M KClO_4 [52]. (ii) Petrii et al. estimated $E_{\text{pzc}} \approx 0.18 \text{ V}$ for Pd/0.05 M $\text{Na}_2\text{SO}_4 + 0.001 \text{ M H}_2\text{SO}_4$ [53]. (iii) The E_{pzc} of Au(111)/0.1 M $\text{HClO}_4 + 5 \times 10^{-3} \text{ M K}_2\text{SO}_4$ assumes a value approximately 0.09 V more negative than in bare 0.1 M HClO_4 . (iv) the E_{pzc} in Au(111-20 nm)/0.1 M H_2SO_4 is estimated to 0.55 V [41,54]. (v) The potential of zero total charge [55], E_{pztc} , of 1 ML Pd–Pt(111) is approximately 0.09 V more negative for specifically adsorbed (hydrogen-) sulphate in 0.1 M H_2SO_4 , in comparison to 0.1 M HClO_4 [11,12].

As the potential advances to more positive values, at $E \geq 0.20$ V negative going bands start to appear at 3440 cm^{-1} and at 1616 cm^{-1} . These bands are assigned to OH-stretching (ν_{OH1}) and HOH-bending (δ_{HOH1}) modes of weakly hydrogen bonded interfacial water [41,54,56–59]. The negative sign of these bands indicates that the amounts of the adsorbed species decrease with respect to the reference spectrum at 0.17 V. Their intensities are continuously increasing in negative direction until saturation is reached at approximately $E \approx 0.40$ V. The peak position of δ_{HOH1} is rather independent of the electrode potential in $0.10\text{ V} < E < 0.80\text{ V}$, while ν_{OH1} changes to slightly higher values. At $E \geq 0.25$ V a new positive going band appears at 1090 cm^{-1} . This band is attributed to the ν_{SO} mode of adsorbed sulphate species [12,41,54]. The peak position of this band shifts at more positive potentials to higher wavenumbers.

Simultaneously with the adsorption of sulphate a broad, positive going band starts to appear at $\nu_{\text{OH2}} \sim 3150\text{ cm}^{-1}$. Band shape and position suggest the formation of strongly hydrogen bonded interfacial water, co-adsorbed with sulphate [41,54,58]. The corresponding δ_{HOH2} band was too weak to be detected within the potential region of an ideally polarised Pd–Au(111–20 nm) electrode. Surface oxidation of Pd starts to interfere at $E > 0.80$ V. Nevertheless, this limited potential range and the low values of ν_{OH2} demonstrate that water interacts stronger with Pd than with the bare gold surface [59]. The quantitative deconvolution and the more detailed interpretation of the complex spectra, as plotted in Fig. 5, will require systematic spectroelectrochemical investigations of Au(111–20 nm) with variable, but defined Pd coverages to approach bulk Pd properties, and the direct comparison with double layer characteristics of well-defined Pd(*hkl*) massive single crystals in contact with 0.1 M H_2SO_4 . This work is still in progress and will be reported elsewhere [60].

3.3.2. Sulphate adsorption

A more detailed analysis of the anion adsorption shows that (hydrogen) sulphate starts to adsorb just in the potential range of the characteristic pair of peaks P2/P2' (Fig. 6). The integrated intensity of the ν_{SO} vibration increases

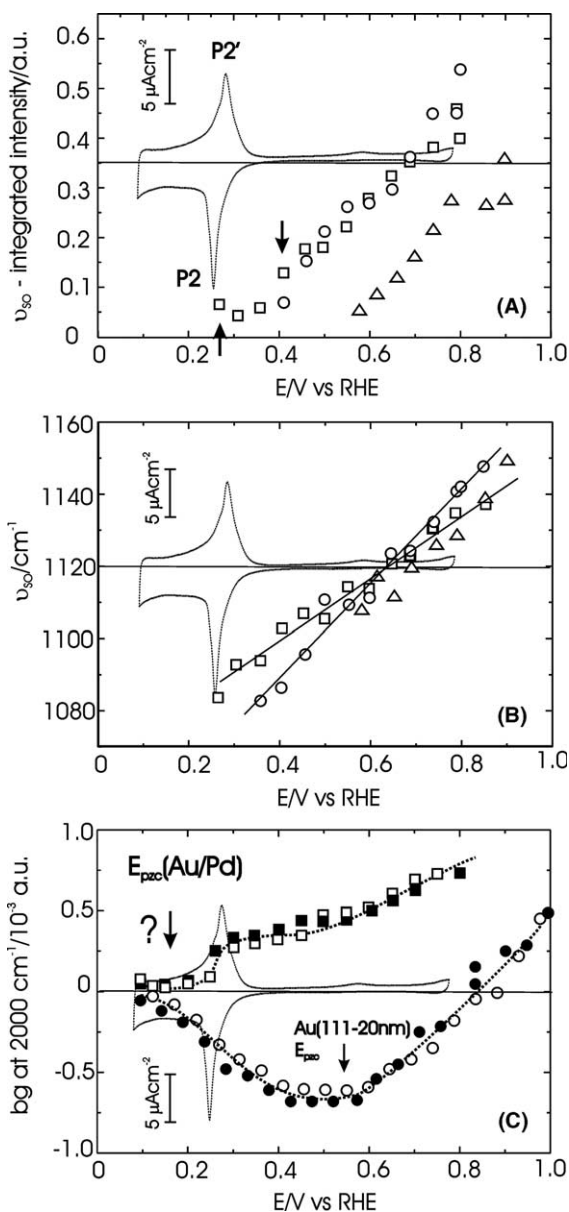


Fig. 6. Plots of the integrated intensities (A), and of the peak positions (B) of the ν_{SO} mode of the adsorbed sulphate species for Au(111–20 nm)/0.1 M H_2SO_4 (○) + 1 ML Pd (□) and 1 ML Pd + CO (Δ) as a function of potential. (C) illustrates the potential dependence of the intensity of the non-resonant background signal at $\nu = 2000\text{ cm}^{-1}$ for the bare gold surface in the absence (○, ●) and in the presence (□, ■) of 1 ML Pd as extracted from SEIRA spectra such as shown in Fig. 5 during a positive (○, □) and a negative going potential scan, respectively. For comparison, the current–potential curve of 1 ML Pd–Au(111–20 nm)/0.1 M H_2SO_4 is also added, scan rate 5 mV s^{-1} .

with more positive potential (Fig. 6A). However, the rise is not as abrupt as found for 1 ML Pd–Pt(111)/0.1 M H₂SO₄ [12], and does not reach a broad potential range of saturation. Simultaneously, the peak position shifts to higher wavenumbers with $\delta\nu_{\text{SO}}/\delta E = 85 \pm 10 \text{ cm}^{-1}\text{V}^{-1}$. This value is smaller than for the disordered (hydrogen) sulphate, $132 \pm 10 \text{ cm}^{-1}\text{V}^{-1}$, but slightly larger than reported for the ordered ($\sqrt{3} \times \sqrt{7}$) sulphate adlayer on the Pd-free Au(111-20 nm) electrode, $63 \pm 3 \text{ cm}^{-1}\text{V}^{-1}$ [41,54]. It is important to note that sulphate adsorbs on the Pd-modified electrode at more negative potentials than on the bare gold surface (cf. arrows in Fig. 6A). The absolute wavenumbers of ν_{SO} in the present experiment and for Au(111-20 nm)/0.1 M H₂SO₄ are rather close and approximately 100 cm^{-1} lower than the data obtained for 1 ML Pd–Pt(111)/0.1 M H₂SO₄ [12]. These observations demonstrate that the gold film template still influences the double layer properties of the Pd-modified electrode.

3.3.3. Non-resonant IR-background

A second interesting result is derived from the IR-nonresonant background, which is represented here by the signal intensity of the IR-baseline at 2000 cm^{-1} . In the absence of enhanced IR-bands, e.g. without absorption from molecular vibrations, the reflectivity changes of an electrode or its representation in the absorbance scale as $-\log(I/I_0)$ are determined primarily by the optical constants (refractive indices) of the substrate and of the adsorbed species [33,35,61]. Changes of the background reflectivity in the present experimental approach represent predominantly the optical properties of the metal electrode, which are potential-dependent, since the refractive indices of palladium and gold are significantly larger in the mid-IR region (Pd: 3.56–17.3i at 2420 cm^{-1} [62]; Au: 3.27–35.21i at 2000 cm^{-1} [63]) than the typical values for water (1.30–1.35 [64]).

We demonstrated before, that the potential dependent background reflectivity at 2000 cm^{-1} for the bare Au(111-20 nm) film electrode in contact with 0.1 M H₂SO₄ as well as for other typical aqueous electrolytes exhibits a parabolic shape with a clearly developed minimum around E_{pzc} (Fig. 6C) [47,60]. Significant changes occur upon

deposition of 1 ML Pd. A shallow new minimum develops around 0.10–0.20 V, followed by a sharp increase of the background signal in the potential region of peak P2/P2', and a further, but continuous increase at higher potentials accompanied by the specific adsorption of sulphate species. No significant hysteresis is observed in $0.10 \text{ V} \leq E \leq 0.80 \text{ V}$. The extension of these measurements towards more negative potentials is hampered by the onset of hydrogen evolution. Despite this limited potential range, the trends in the potential dependence of the baseline intensity of “free” and Pd-modified Au(111-20 nm) film electrodes in 0.1 M H₂SO₄ strengthen the assumption introduced at the beginning of this paragraph, that E_{pzc} of the latter system is located around 0.10–0.20 V. Additional support for this hypothesis will be given in experiments with variable Pd adlayer coverages approaching bulk Pd properties [60].

3.4. CO-adsorption and oxidation on quasi single crystalline gold film electrodes modified with 1 ML Pd in 0.1 M H₂SO₄

3.4.1. Adsorption

We have chosen the adsorption and electro-oxidation of a saturated CO adlayer to explore additional structural and reactivity properties of the fabricated Pd-modified thin film electrodes in acidic medium. For reference, we investigated first the adsorption of CO on the bare gold surface. Fig. 7 illustrates the evolution of the SEIRA spectra for Au(111-20 nm)/0.1 M H₂SO₄ upon dosing with CO at 0.10 V. The reference spectrum was chosen at $t = 0$. No significant changes were found in the spectral ranges of ν_{OH} and δ_{HOH} modes of interfacial water as well as below 1500 cm^{-1} . Only one positive going band appears at 2109 cm^{-1} , FWHM = $24 \pm 2 \text{ cm}^{-1}$. Maximum intensity is reached under our experimental conditions in CO saturated electrolyte at $t \geq 600 \text{ s}$ (Fig. 7A). Peak position and FWHM do not change with time. This band has been observed before [65–67] and is assigned to the stretching mode of linearly bound CO, $\nu_{\text{COT}}(\text{Au})$. The peak position is much higher than that observed on transition metals (cf. 2080–2050 cm^{-1} on Pt, Pd, Rh) [68] and closer to that of free CO (2143 cm^{-1}) [57] suggesting

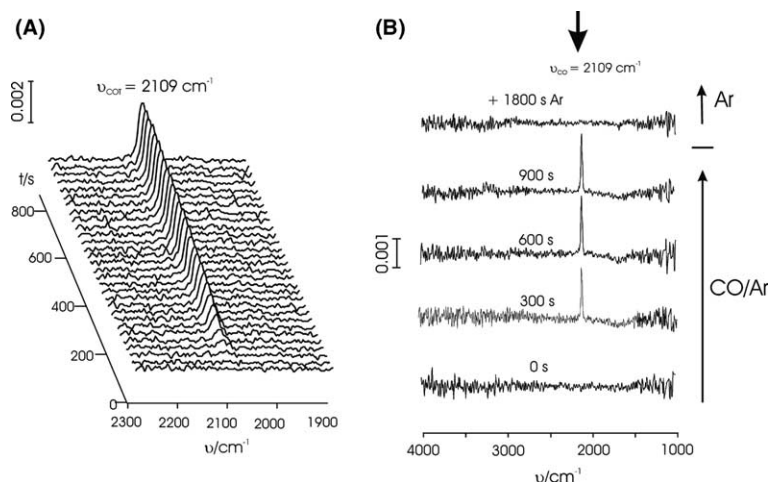


Fig. 7. Time dependent SEIRA spectra for the deposition of CO on Au(111-20 nm)/0.1 M H₂SO₄ at 0.10 V during the continuous purging of the electrolyte with a CO/Ar mixture. The reference spectrum was taken at $t = 0$ s. (A) shows the spectroscopic range from $1900\text{ cm}^{-1} < \nu < 2300\text{ cm}^{-1}$ while (B) illustrates, as examples, selected spectra in $1000\text{ cm}^{-1} < \nu < 4000\text{ cm}^{-1}$ during the CO/Ar exposure and (top spectrum) after extended purging with argon only to remove the CO from the bulk of the electrolyte.

a weak adsorption of CO. Gold, which differs from the transition metals by its electronic configuration of fully occupied d-orbitals ($5d^{10}6s^1$) is indeed expected to exhibit a weaker co-ordination ability for CO. Our interpretation is further supported by the following observations: (i) The adsorption of CO on Au(111-20 nm) does not change the intensity of the nonresonant IR-background signal. The latter is rather sensitive to strong physisorption and chemisorption [69]. (ii) Careful purging with Ar for at least 30 min to remove bulk solution CO is accompanied with the quantitative desorption of interfacial CO (Fig. 7B).

Subsequently we deposited CO onto Au(111-20 nm) modified with 1 ML Pd at 0.10 V, and carried out a “spectroelectrochemical charge displacement” experiment. At the potential chosen all Pd-sites are covered with atomic hydrogen and no anions are adsorbed. Fig. 8 illustrates a series of time-dependent SEIRA spectra, which was recorded simultaneously with the corresponding electrochemical $i-t$ transient (Fig. 9A). The experimental conditions ensured the formation of a saturated CO adlayer, which most probably exhibits no long range order [70]. The voltammetric current is completely blocked in $0.10\text{ V} \leq E \leq 0.75\text{ V}$. The measured spectra are dis-

tinctly different from those recorded for the bare Au(111-20 nm) film electrode in contact with 0.1 M H₂SO₄ (Fig. 7). Characteristic positive going bands evolve in the regions of OH- and CO-stretching. No anion-related modes were found. The CO vibrations are readily distinguished at 2106 cm^{-1} (FWHM = $24 \pm 1\text{ cm}^{-1}$), 2052 cm^{-1} (FWHM = $35 \pm 2\text{ cm}^{-1}$) and 1930 cm^{-1} (FWHM = $44 \pm 2\text{ cm}^{-1}$). The time dependence of the corresponding integral intensities, of the peak positions and of the IR-background signal at 2300 cm^{-1} during CO dosing and subsequent Ar purging are plotted in Fig. 9B–D. This analysis neglects possible intensity transfer due to dipole–dipole coupling within the CO adlayer [71]. The inspection of Figs. 8 and 9C reveals that the high frequency mode disappears after ca. 30 min upon treatment of the electrolyte with bare Ar. This temporary band is attributed to atop CO physisorbed on the still remaining “free” gold sites ($\nu_{\text{CO-T}}(\text{Au})$, cf. Fig. 7). A rough estimation, based on the integrated CO intensities of Fig. 9C, suggests that in these experiments typically more than 90% of the gold electrode area are covered with a monolayer of Pd.

Based on IRAS data of CO adsorption on Pd(111), Pd–Au(111) or Pd–Pt(111) in UHV [72–76] and under electrochemical conditions in

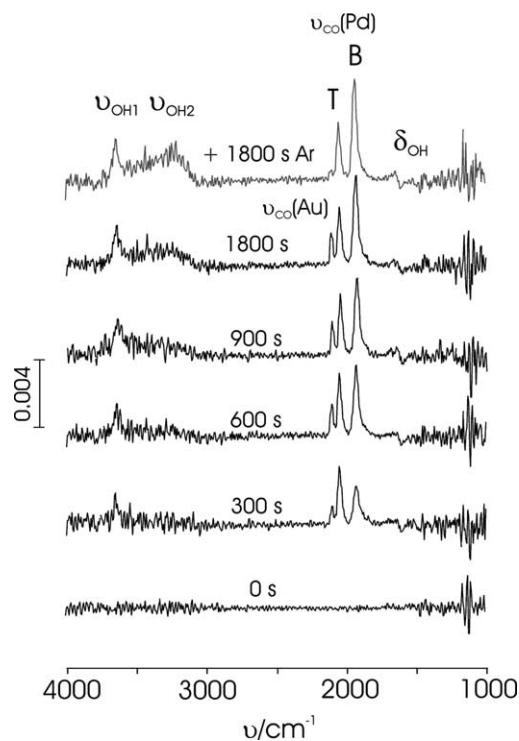


Fig. 8. Time dependent in situ SEIRA spectra for the deposition of CO on 1 ML Pd–Au(111-20 nm)/0.1 M H₂SO₄ at 0.10 V during the continuous exposure of the electrolyte to a CO/Ar mixture (black lines) and after extended purging with Ar only (grey lines). A set of single scan spectra measured at $t = 0$ in the absence of CO was chosen as reference.

solution [6,14,43,77] we assign the low frequency mode to chemisorbed, bridge bonded CO on Pd, which we will abbreviate in the following as $\nu_{\text{COB}}(\text{Pd})$. The slight asymmetry of this band with an extended tail region toward lower wavenumbers suggests contributions from edge and terrace sites [14]. The remaining third CO vibration at $\sim 2052 \text{ cm}^{-1}$ is attributed to atop CO adsorbed at step sites on the Pd surface and will be labelled $\nu_{\text{COT}}(\text{Pd})$. This interpretation is based on a comparison of our experimental observations with published IRAS and SERS studies employing size- and shape-controlled Pd-nanoparticles [78–80], Pd multilayers [81,82] or Au–Pd alloy films of defined composition [83]. Chemisorption of CO is clearly represented by the increase of the nonresonant IR-background intensity until saturation is reached at $t \geq 30 \text{ min}$ (Fig. 9B). In comparison

to SEIRAS experiments measured with CO on sputtered [37] or electrochemically deposited Pt films [36] we did not observe bipolar bands.

The temporary evolution of the interfacial CO vibrations at 0.10 V (Fig. 9C and D) reveals that $\nu_{\text{COT}}(\text{Au})$ and $\nu_{\text{COT}}(\text{Pd})$ reach their maximum at $\sim 400 \text{ s}$ while $\nu_{\text{COB}}(\text{Pd})$ rises further. At low coverages, CO adsorbs preferentially at step sites. A steady state spectroscopic response is reached after Ar purging of the electrolyte accompanied by the complete removal of physisorbed CO from Au sites. Simultaneously with these CO vibrations one observes in the OH stretching region positive going bands, one, $\nu_{\text{OH1}} \approx 3642 \pm 4 \text{ cm}^{-1}$, is sharp and the other, $\nu_{\text{OH2}} \approx 3250 \pm 10 \text{ cm}^{-1}$, is rather broad (Fig. 8). The corresponding δ_{HOH} bending vibrations are present, but too weak to be quantitatively resolved. Nevertheless, since CO is hydrophobic and the sharp OH stretching band appears at high CO coverages, these spectral features indicate the coadsorption of CO with isolated interfacial water and with second layer hydrogen bonded water [47,56–58]. The presence of stabilising interfacial water in high coverage CO adlayers was already hypothesised for Pd(111)/CO from IRAS [43,84] and UHV emersion experiments [85]. Zhu et al. concluded, based on high energy electron energy loss spectroscopy (HREELS) in combination with temperature programmed desorption (TPD) for the competitive adsorption of water and CO on Pd(111) that (i) CO blocks water adsorption sites and (ii) facilitates the formation of second layer (secondary) hydrogen bonded water [86]. However, the data plotted in Figs. 8 and 9 represent, to the best of our knowledge, the first real time in situ spectroelectrochemical study of structural changes within the Helmholtz layer during a so-called CO charge displacement experiment. We also like to point out, that the time constant of the spectroscopic response is significantly higher than that of the simultaneously recorded electrochemical $i-t$ transient. One important consequence of these results comprises the critical evaluation of the “classical” charge displacement experiment, which was usually analysed according to the following dominant mechanisms [87]:



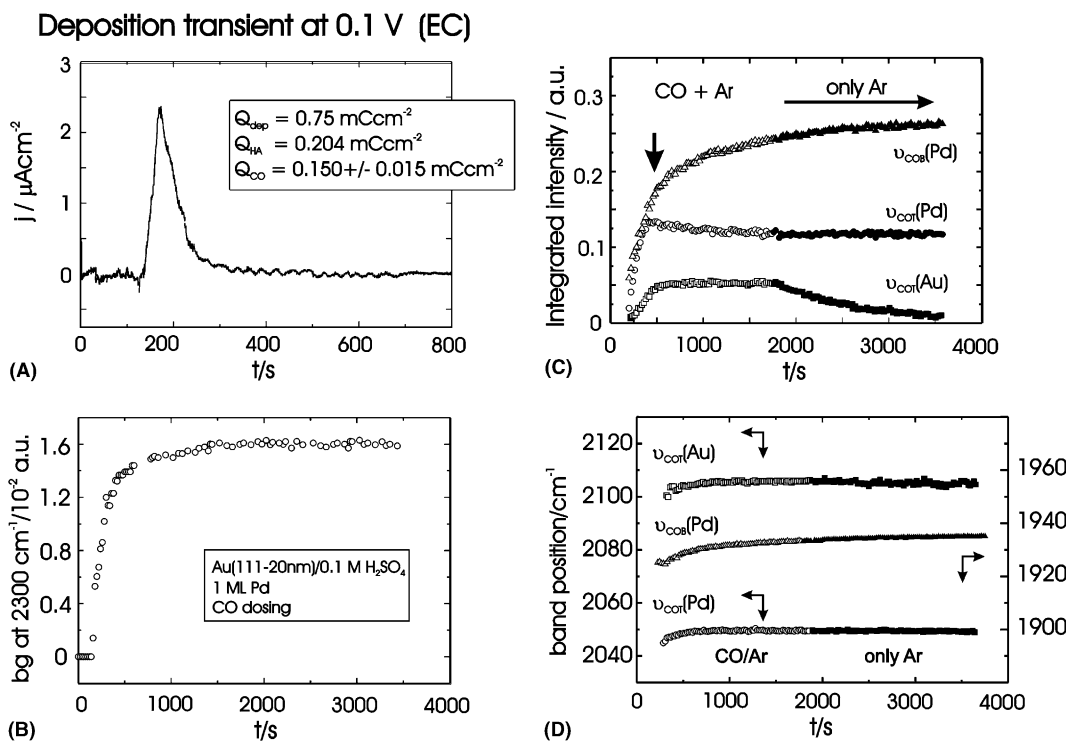
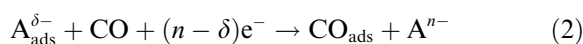


Fig. 9. (A) Simultaneously with the spectral response (Fig. 8) monitored “charge displacement” transient for the deposition of CO on 1 ML Pd–Au(111-20 nm)/0.1 M H₂SO₄ at 0.10 V, and the time dependent evolution of the background intensity at 2300 cm⁻¹ (B), of the integrated intensities (C) and of the band positions (D) of the observed CO stretching modes $\nu_{\text{COT}}(\text{Au})$, $\nu_{\text{COT}}(\text{Pd})$, $\nu_{\text{COB}}(\text{Pd})$.



This will be the topic of a forthcoming publication, where the potential and coverage dependence of simultaneously recorded spectroscopic and electrochemical charge displacement transients will be quantitatively analysed, and compared with the corresponding single crystal data [60].

3.4.2. Oxidation

After the formation of a steady state saturated CO adlayer at 0.10 V on 1 ML Pd–Au(111-20 nm) and complete removal of bulk solution CO we employed a slow potential scan, 2.5 mV s⁻¹, to monitor in situ the potential dependence of CO electro-oxidation (Fig. 10). The current–potential curve (Fig. 10A) reveals that the hydrogen adsorption is suppressed completely and the currents remain close to zero until $E \approx 0.75$ V. At higher potentials a rather sharp peak P1 devel-

ops with a maximum at $E = 0.86$ V. Further oxidation of the CO adlayer gives rise to a second peak P2 at $E = 1.02$ V. Reversing the electrode potential just after passing P1 causes incomplete electro-oxidation of adsorbed CO, accompanied with the partial reappearance of the typical features for the hydrogen adsorption region I. However, if the CO oxidation is extended to $E > 1.02$ V the following potential scan and the characteristic hydrogen states appear rather distorted. The data shown in Fig. 10A demonstrate that CO oxidation on 1 ML Pd–Au(111-20 nm) electrodes proceeds in two distinct potential regions. The comparison of our observations with recent data for CO-oxidation on stepped Au(*hkl*) surfaces modified with thin Pd films [29] suggests the assignment of the potential region around P1 to CO adsorption on defect (preferentially step) sites, while the more positive feature P2 is attributed to the reaction at terraces having a certain size. The latter process

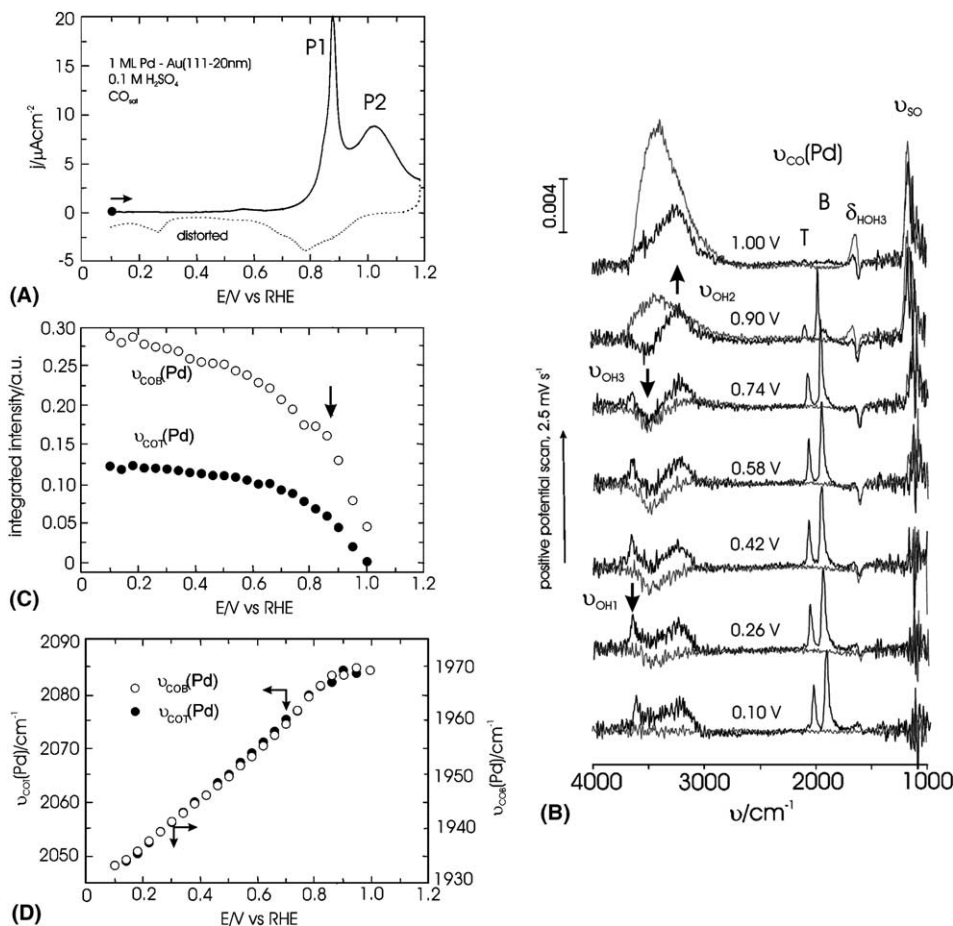


Fig. 10. (A) shows the current–potential curve in $0.10 \text{ V} < E < 1.18 \text{ V}$ (solid black line, 2.5 mV s^{-1}). The “distorted” negative-going scan is shown as dotted line. The grey traces represent the bare supporting electrolyte without Pd and CO. (B) Evolution of the SEIRA spectra for the electro-oxidation of a saturated CO adlayer deposited at 0.10 V on $1 \text{ ML Pd-Au}(111-20 \text{ nm})/0.1 \text{ M H}_2\text{SO}_4$ during a slow positive going potential scan and in the absence of bulk electrolyte CO. (C) and (D) illustrate the potential dependent evolution of the CO modes.

is superimposed with the partial oxidative dissolution of Pd accompanied by an irreversible increase of surface defects. We also like to point out that these voltammetric data indicate that CO oxidation on Pd–Au(111-20 nm) and Pd–Au(111) electrodes in $0.1 \text{ M H}_2\text{SO}_4$ [29] proceeds with a lower rate than on ideal Pt(111) [11,12] and stepped Pt(*hkl*) [88–90] surfaces, despite the higher affinity of Pd to oxygen-containing species [7]. The oxygen-containing species appears to be not easily transferred to adsorbed CO.

The simultaneously recorded SEIRA spectra for CO oxidation on $1 \text{ ML Pd-Au}(111-20 \text{ nm})/$

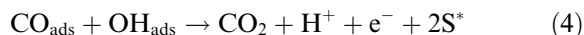
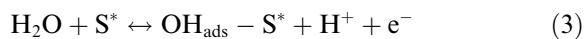
$0.1 \text{ M H}_2\text{SO}_4$ are shown in Fig. 10B (black lines). The reference spectrum was chosen at 0.10 V in the absence of CO. The grey traces represent the response of the bare Au(111-20 nm) surface in $0.1 \text{ M H}_2\text{SO}_4$. Advancing the electrode potential towards more positive values reveals distinct changes in four spectral regions representing CO- and OH-stretching modes, HOH-bending and anion-related vibrations at $\nu < 1200 \text{ cm}^{-1}$ (Fig. 10B). The intensities of linear and bridge bonded CO, $\nu_{\text{COI}}(\text{Pd})$ and $\nu_{\text{COB}}(\text{Pd})$, start to decrease already at potentials slightly larger than 0.10 V in the so-called pre-oxidation region (cf. discussion for CO

electro-oxidation on Pt(111) in Ref. [91]). A major and rather abrupt decrease occurs around the peak P1 of the simultaneously measured current–potential curve, which was previously assigned to CO oxidation on defect sites. No CO related signals were detected at $E > 1.06$ V. We note that the contribution of $\nu_{\text{COT}}(\text{Pd})$ vanishes at lower electrode potentials than that of $\nu_{\text{COB}}(\text{Pd})$ (Fig. 10C). Both vibration modes exhibit a rather similar tuning rate $\delta\nu/\delta E = 45 \pm 2 \text{ cm}^{-1}\text{V}^{-1}$, deviations exist only around the oxidation peak P1. This value corresponds reasonably with literature data for CO on Pd(111) ($\delta\nu_{\text{COB}}/\delta E = 35 \text{ cm}^{-1}\text{V}^{-1}$ [43]) and CO on Pd–Pt(111) ($\delta\nu_{\text{COB}}/\delta E = 35 \text{ cm}^{-1}\text{V}^{-1}$ or $50 \text{ cm}^{-1}\text{V}^{-1}$ [14]), respectively. The blue shift is attributed to the superposition of the electrochemical Stark effect [92] with contributions due to redistribution of charges within the CO molecule [93] and dipole–dipole coupling [68,69]. The linear dependence of ν on E also indicates that the structural changes within the adlayer at $E < E(\text{P1})$ do not seem to modify the local environment of the adsorbed CO species dramatically! This interpretation is supported by the estimated values of the FWHM, $35 \pm 2 \text{ cm}^{-1}$ ($\nu_{\text{COT}}(\text{Pd})$) and $45 \pm 3 \text{ cm}^{-1}$ ($\nu_{\text{COB}}(\text{Pd})$), which do not change with potential until E approaches 1.00 V.

The OH-stretching (ν_{OH}) and HOH-bending (δ_{HOH}) modes of interfacial water are observed at $3700\text{--}3000 \text{ cm}^{-1}$ and at $1650\text{--}1610 \text{ cm}^{-1}$, respectively. One may readily distinguish three OH-stretching modes. However, their quantitative deconvolution is not straightforward at the present stage of our knowledge. Therefore, we restrict the following description and analysis to a qualitative level choosing the CO-free spectrum at $E = 0.10$ V as reference state (cf. Section 3.3). The intensity of the high frequency vibration ν_{OH1} , previously already assigned to isolated water, decreases with more positive potentials and vanishes at $E < 0.90$ V, e.g. just past the voltammetric peak P1 (Fig. 10A), indicating that these water species are destabilized and/or being directly involved in the electro-oxidation of CO. Simultaneously, a negative going band appears around 3480 cm^{-1} , ν_{OH3} , which can be attributed to the continuous loss of weakly hydrogen-bonded interfacial water [54,56–58]. The corresponding HOH-bending

mode, δ_{HOH3} , is found at $1614 \pm 2 \text{ cm}^{-1}$. These water features correlate with the potential dependent evolution of the CO-stretching modes, $\nu_{\text{COT}}(\text{Pd})$ and $\nu_{\text{COB}}(\text{Pd})$, and indicate that both water species are involved in the electro-oxidation of atop and bridge bonded CO. Atop CO at defect sites ($\nu_{\text{COT}}(\text{Pd})$) appears to be consumed preferentially. The third OH-vibration, ν_{OH2} , which was assigned to second layer hydrogen bonded water, is rather unperturbed by these changes until, at $E \geq 0.55$ V, sulphate species (ν_{SO} , Fig. 6A) start to adsorb on sites of the Pd–Au(111–20 nm) surface, where CO was already desorbed due to the onset of electro-oxidation. The begin of the (hydrogen-) sulphate adsorption is inhibited by the presence of adsorbed CO, and appears at approximately 0.30 V more positive with reference to the CO-free system 1 ML Pd–Au(111–20 nm)/0.1 M H_2SO_4 (Fig. 6A). The increasing surface excess of (hydrogen-) sulphate facilitates the co-adsorption of hydrogen-bonded interfacial water, which is represented by an intensity increase and a slight blue shift of ν_{OH2} , especially pronounced at $E > 0.90$ V, where the CO coverage drops dramatically.

The potential dependent evolution of the simultaneously monitored vibrational modes of interfacial CO and water species support the “reactant pair” mechanism of electro-oxidation of adsorbed CO in acidic medium, originally proposed by Gilman [94]:



where S^* denotes a free surface site.

This mechanism assumes a Langmuir–Hinshelwood type reaction between CO and a surface oxygen-containing species, adsorbed on adjacent sites, to form CO_2 (not detected in the SEIRA spectrum due to the desorption into the bulk of the electrolyte, which differs from IRAS results in “thin layer configuration” [33,68]!). The potential-dependent evolution of the vibrational modes attributed to interfacial water species suggests that the oxygen-containing species could be co-adsorbed isolated and/or weakly hydrogen-bonded interfacial water.

4. Summary and conclusions

(1) In this study we have prepared and characterized quasi single crystalline gold film electrodes of 20 nm thickness and preferential (111) surface orientation by electron beam evaporation onto a Si hemisphere in combination with electrochemical annealing. These samples were subsequently modified with ultrathin layers (sub-ML, ML, multi-L) of Pd employing a potentiostatic deposition regime. Similar to previous reports for Pd on massive Au(111) single crystals, we could demonstrate that the deposition of the first Pd ML onto Au(111-20 nm) starts at underpotentials. We observed well developed current peaks of hydrogen adsorption/(hydrogen) sulphate desorption (and of the respective anodic counter parts) on first and multilayer Pd. Comparing the charges of the characteristic hydrogen/anion “states”, Q_{HA} , with the deposited amount of Pd from sulphate- and/or chloride-containing electrolyte, Q_{Pd} , results in a “calibration master curve” with two distinct slopes and an intersection point at $Q_{\text{Pd}} = 0.72 \pm 0.08 \text{ mCcm}^{-2}$ and $Q_{\text{HA}} = 0.20 \pm 0.02 \text{ mCcm}^{-2}$. Based on these data and taking into consideration the scaling factor of 1.6, which represents the ratio between the electrochemically active and the geometrical area of our template films, we could establish conditions to fabricate defined and stable Pd monolayers on Au(111-20 nm).

(2) In situ ATR-SEIRAS experiments with 1 ML Pd–Au(111-20 nm) electrodes demonstrated for the first time that enhanced IR signals of physisorbed and chemisorbed species can be obtained on *well defined* and catalytically active Pt-group model electrodes. Our approach is based on the controlled modification of a SEIRAS-active, quasi single crystalline gold template. We compared the potential-dependent properties of interfacial water and adsorbed (hydrogen) sulphate on Au(111-20 nm)/0.1 M H₂SO₄ in the absence and in the presence of 1 ML Pd. We found that weakly hydrogen bonded water is replaced by strongly hydrogen bonded interfacial water accompanied by an increasing amount of adsorbed (hydrogen) sulphate if the potential advances to more positive values. The onset of adsorption of the sulphate species appears to be at more negative potentials

on Pd–Au(111-20 nm), in comparison to the bare gold surface. Analysing the potential dependence of the non-resonant IR background signal (at 2000 cm⁻¹) we observed distinct differences between both electrodes, and suggested that the E_{pzc} of 1 ML Pd–Au(111-20 nm)/0.1 M H₂SO₄ is located around 0.10–0.20 V (vs. RHE).

(3₁) The adsorption and electro-oxidation of CO were chosen as test processes to probe structural and reactivity properties of the fabricated Pd-modified thin film electrodes. Reference experiments with Au(111-20 nm)/0.1 M H₂SO₄ revealed that CO is weakly physisorbed from CO-saturated electrolyte giving rise to a characteristic band, $\nu_{\text{CO-T}}(\text{Au})$, at 2109 cm⁻¹, which could be assigned to the stretching mode of linearly bound CO. However, complete desorption was found in CO-free electrolyte after prolonged purging with argon.

(3₂) Simultaneous spectroelectrochemical (time-resolved in situ ATR-SEIRAS) and electrochemical “charge displacement” experiments were carried out to monitor the deposition of a saturated CO adlayer on 1 ML Pd–Au(111-20 nm)/0.1 M H₂SO₄ at 0.10 V. The measured spectra are distinctly different from those recorded for the bare gold film. Characteristic positive going bands evolve in the regions of OH- and CO-stretching, which could be assigned to isolated water ($\nu_{\text{OH1}} \sim 3642 \text{ cm}^{-1}$) and second layer, hydrogen bonded water ($\nu_{\text{OH2}} \sim 3250 \text{ cm}^{-1}$) co-adsorbed with chemisorbed CO on Pd at bridge sites ($\nu_{\text{COB}}(\text{Pd})$) and in atop positions at step edges ($\nu_{\text{COT}}(\text{Pd})$). The temporarily detected band $\nu_{\text{CO-T}}(\text{Au})$ (before removing CO from the bulk of the electrolyte) allowed us to estimate the still remaining “free gold sites” for 1 ML Pd–Au(111-20 nm) to be less than 10% of the active electrode area. The time dependent evolution of the $i-t$ and of the spectroscopic charge displacement transients revealed that the structural changes of the adlayer are taking place at a much longer time scale than one might assume, just based on the electrochemical data. These results suggest the need for a critical re-evaluation of the “classical” charge displacement experiment, a topic that we intend to address in a separate communication.

(3₃) We presented in this paper also the first in situ ATR-SEIRAS experiments for the electro-

oxidation of adsorbed CO on 1 ML Pd–Au(111–20 nm)/0.1 M H₂SO₄. Our approach allowed recording simultaneously the potential dependent evolution of vibration modes of adsorbed CO and anions as well as of interfacial water species. We provide evidence that co-adsorbed, isolated and weakly hydrogen bonded interfacial water are disordered and eventually consumed during the electro-oxidation of CO, and that atop CO on defect sites appears to react first. The “CO-free” surface spots will be subsequently covered by (hydrogen-) sulphate which, in addition, facilitates the co-adsorption of hydrogen bonded water. These spectroscopic observations are consistent with the “reactant pair” mechanism of electro-oxidation of CO in acidic medium, and provide new insight into structural changes within the adlayer during the course of the reaction.

(34) The ability to fabricate *well defined*, SEIRAS-active Pd–Au(111–20 nm) model electrodes for in situ spectroscopic and electrochemical studies demonstrates the unique chance and opportunity to apply the advantages of in situ ATR-SEIRAS in terms of sensitivity, time resolution and mass transport to (electro-) catalytic applications with *well defined* Pt-group substrates to develop detailed and novel structure–reactivity correlations. The presented approach may also provide new insight into the double layer properties of “reactive” materials in contact with aqueous electrolytes. Both topics will be addressed in our future research program with major focus on extending the present “demonstration studies” with Pd–Au(111–20 nm) to other Pt-type materials employing spatial as well as time resolved approaches.

Acknowledgments

S.P. is indebted to the Alexander von Humboldt Foundation for a Research Fellowship. The authors would like to thank Mr. Bierfeld and B. Han for support in operating the evaporation chamber. We also like to thank Juan Feliu and Bob de Levie for many valuable comments. The work was also supported by the Research Center Jülich under contract E2910201.

References

- [1] D.M. Kolb, Surf. Sci. 500 (2000) 722.
- [2] D.M. Kolb, in: R.C. Alkire, D.M. Kolb (Eds.), *Advances in Electrochem. Sci. & Eng.*, vol. 7, Wiley–VCH, Weinheim, 2000, p. 107.
- [3] R.R. Adzic, in: E. Gileadi, M. Urbakh (Eds.), *Encyclopedia of Electrochemistry*, vol. 1, Wiley–VCH, Weinheim, 2002, p. 561.
- [4] A. Ruban, B. Hammer, P. Stoltze, H.L. Skiver, J.K. Norskov, J. Mol. Catal. A 115 (1997) 421.
- [5] G. Attard, A. Bannister, J. Electroanal. Chem. 300 (1991) 467.
- [6] J. Inukai, M. Ito, J. Electroanal. Chem. 358 (1993) 307.
- [7] M.J. Llorca, J.M. Feliu, A. Aldaz, J. Clavilier, J. Electroanal. Chem. 351 (1993) 299.
- [8] M. Baldauf, D.M. Kolb, J. Phys. Chem. 100 (1996) 11375.
- [9] R. Gomez, A. Rodes, M. Perez, J.M. Feliu, A. Aldaz, Surf. Sci. 327 (1995) 202; Surf. Sci. 344 (1995) 85.
- [10] N.M. Marcovic, C.A. Lucas, V. Climent, V. Stamenovic, P.N. Ross, Surf. Sci. 465 (2000) 103.
- [11] B. Alvarez, V. Climent, A. Rodes, J.M. Feliu, Phys. Chem. Chem. Phys. 3 (2001) 3269.
- [12] B. Alvarez, V. Climent, A. Rodes, J.M. Feliu, J. Electroanal. Chem. 497 (2001) 125.
- [13] M. Arenz, V. Stamenovic, T.J. Schmidt, K. Wandelt, P.N. Ross, N.M. Marcovic, Surf. Sci. 506 (2002) 287.
- [14] B. Alvarez, A. Rodes, J.M. Perez, J.M. Feliu, J. Phys. Chem. B 107 (2003) 2018.
- [15] M. Baldauf, D.M. Kolb, Electrochim. Acta 38 (1993) 2145.
- [16] H. Naohara, S. Ye, K. Uosaki, J. Phys. Chem. B 102 (1998) 4366.
- [17] H. Naohara, S. Ye, K. Uosaki, J. Electroanal. Chem. 473 (1999) 2.
- [18] H. Naohara, S. Ye, K. Uosaki, Colloids Surf. A 154 (1999) 201.
- [19] L.A. Kibler, M. Kleinert, R. Randler, D.M. Kolb, Surf. Sci. 443 (1999) 19.
- [20] L.A. Kibler, M. Kleinert, D.M. Kolb, Surf. Sci. 461 (2000) 155.
- [21] H. Naohara, S. Ye, K. Uosaki, Electrochim. Acta 45 (2000) 3305.
- [22] M. Takahashi, Y. Hayashi, J. Mizuki, K. Tamura, T. Kondo, H. Naohara, K. Uosaki, Surf. Sci. 461 (2000) 213.
- [23] H. Naohara, S. Ye, K. Uosaki, J. Electroanal. Chem. 500 (2001) 435.
- [24] M.E. Quayum, S. Ye, K. Uosaki, J. Electroanal. Chem. 520 (2002) 126.
- [25] L. Kibler, M. Kleinert, V. Lazarescu, D.M. Kolb, Surf. Sci. 498 (2002) 175.
- [26] L.A. Kibler, A.M. El-Aziz, D.M. Kolb, J. Mol. Catal. A 199 (2003) 57.
- [27] B. Alvarez, V. Climent, J.M. Feliu, A. Aldaz, Electrochem. Commun. 2 (2000) 427.
- [28] A.M. El-Aziz, L.A. Kibler, D.M. Kolb, Electrochem. Commun. 4 (2002) 535.

- [29] A.M. El-Aziz, L.A. Kibler, *J. Electroanal. Chem.* 534 (2002) 107.
- [30] S.R. Brankovic, J.X. Wang, R.R. Adzic, *Surf. Sci.* 474 (2001) L173.
- [31] M. Mavrikakis, B. Hammer, J.K. Nørskov, *Phys. Rev. Lett.* 81 (1998) 2819.
- [32] A. Roudar, A. Groß, *Phys. Rev. B* 67 (2003) 033409.
- [33] M. Osawa, *Bull. Chem. Soc. Jpn.* 70 (1997) 2861.
- [34] M. Osawain, S. Kawata (Eds.), *Topics Appl. Phys.* 81 (2001) 185.
- [35] W. Suetaka, *Surface Infrared and Raman Spectroscopy—Methods and Applications*, Plenum Press, New York, 1995.
- [36] A.E. Bjerke, P.R. Griffiths, W. Theiss, *Anal. Chem.* 71 (1999) 1967.
- [37] Y. Zhu, H. Uchida, M. Watanabe, *Langmuir* 15 (1999) 8757.
- [38] A. Miki, S. Ye, M. Osawa, *Chem. Commun.* (2002) 1500.
- [39] M. Watanabe, Y. Zhu, H. Uchida, *J. Phys. Chem. B* 104 (2000) 1762.
- [40] Y.X. Chen, A. Miki, S. Ye, H. Sakai, M. Osawa, *J. Am. Chem. Soc.* 125 (2003) 3680.
- [41] Th. Wandlowski, K. Ataka, S. Pronkin, D. Diesing, *Electrochim. Acta* 49 (2004) 1233.
- [42] L. Kibler, M. Baldauf, D.M. Kolb, in: J. Garce (Ed.), *Electrochemie für Energie und Umwelt*, Universitätsverlag, Ulm, 1997, p. 63.
- [43] S. Zhou, R. Gomez, M.J. Weaver, *J. Electroanal. Chem.* 474 (1999) 155.
- [44] N. Hoshi, K. Kagaya, Y. Hori, *J. Electroanal. Chem.* 485 (2000) 55;
N. Hoshi, M. Kuroda, Y. Hori, *J. Electroanal. Chem.* 521 (2002) 155.
- [45] S. Strbec, R.R. Adzic, A. Hamelin, *J. Electroanal. Chem.* 249 (1988) 291.
- [46] D. Mayer, K. Ataka, Th. Wandlowski, *J. Electroanal. Chem.*, in preparation, 2004.
- [47] S. Pronkin, Th. Wandlowski, *J. Electroanal. Chem.* 550–551 (2003) 131.
- [48] S. Pronkin, Th. Wandlowski, unpublished, 2003.
- [49] M. Baldauf, Ph.D. Thesis, University of Ulm, 1996.
- [50] L.J. Wan, T. Suzuki, K. Sashikata, J. Okada, J. Inukai, K. Itaya, *J. Electroanal. Chem.* 484 (2000) 189.
- [51] B.E. Koel, A. Sellidj, M.T. Paffett, *Phys. Rev. B* 46 (1992) 7846.
- [52] A.S. Dakkouri, D.M. Kolb, in: A. Wieckowski (Ed.), *Interfacial Electrochemistry*, Plenum Press, New York, 1999, p. 151.
- [53] V. Topolev, O. Petrii, *Elektrochimija* 6 (1970) 852.
- [54] K. Ataka, M. Osawa, *Langmuir* 14 (1998) 951.
- [55] A.N. Frumkin, O.A. Petrii, B.B. Damaski, in: J. O'M Bockris, B.E. Conway, E. Yeager (Eds.), *Comprehensive Treatise of Electrochemistry*, vol. 1, Plenum Press, New York, 1980, p. 221.
- [56] J.R. Scherrer, in: R.J.H. Clark, R.E. Hesters (Eds.), *Advances in Infrared and Raman Spectroscopy*, vol. 5, Heyden, Philadelphia, 1978, p. 151.
- [57] K. Nakamoto, *Infrared and Raman Spectra of Inorganic and Coordination Compounds*, 4th ed., Wiley, New York, 1986.
- [58] P.A. Thiel, T.E. Madey, *Surf. Sci. Rep.* 7 (1987) 211.
- [59] M. Wolf, S. Nettersheim, J.M. White, E. Hasselbrink, G. Ertl, *J. Chem. Phys.* 94 (1991) 4609.
- [60] S. Pronkin, I. Pobelov, Th. Wandlowski, in preparation.
- [61] D. Diesing, S. Pronkin, K. Ataka, Th. Wandlowski, *Phys. Chem. Chem. Phys.*, in preparation.
- [62] J.H. Weaver, R.L. Bendow, *Phys. Rev. B* 12 (1975) 3509.
- [63] G.P. Motulevich, A.A. Shikin, *Sov. Phys. JETP* 20 (1965) 560.
- [64] U. Dummy, in: D.R. Linde (Ed.), *CRC Handbook of Chemistry and Physics*, 71st Ed., CRC, Boca Raton, 1991.
- [65] S. Dennis, S. Corrigan, P. Gao, L.W. Leung, M.J. Weaver, *Langmuir* 2 (1986) 744.
- [66] S.C. Cheng, A. Hamelin, M.J. Weaver, *J. Phys. Chem.* 95 (1991) 5560.
- [67] S.G. Sun, W.B. Cai, L.J. Wan, M. Osawa, *J. Phys. Chem.* 103 (1999) 2460.
- [68] T. Iwasita, F.C. Nart, in: H. Gerischer, C.W. Topias (Eds.), *Advances in Electrochem. Sci. and Engineering*, vol. 4, VCH, Weinheim, 1995, p. 123.
- [69] B.N. Person, *Phys. Rev. B* 44 (1991) 3277.
- [70] C.A. Lucas, N. Markovic, M. Ball, V. Stamenkovic, V. Climent, P.N. Ross, *Surf. Sci.* 479 (2001) 241.
- [71] B.N.J. Persson, M. Tüshaus, A.M. Bradshaw, *J. Chem. Phys.* 92 (1990) 5034.
- [72] A. Sellidj, B.E. Koel, *Phys. Rev. B* 49 (1994) 8367.
- [73] F.M. Hoffmann, *Surf. Sci. Rep.* 3 (1983) 107.
- [74] M. Tüshaus, W. Berndt, H. Conrad, A.M. Bradshaw, B. Person, *Appl. Phys. A* 51 (1990) 91.
- [75] S. Surnev, M. Sock, M.G. Ramsey, F.P. Netzer, M. Wiklund, M. Borg, J.N. Andersen, *Surf. Sci.* 470 (2000) 171.
- [76] A.K. Santraa, D.W. Goodman, *Electrochim. Acta* 47 (2002) 3595.
- [77] M. Arenz, V. Stamenkovic, T.J. Schmidt, K. Wandelt, P.N. Ross, N.M. Markovic, *Surf. Sci.* 506 (2002) 287.
- [78] K. Walter, O. Seiffert, H. Kuhlbeck, M. Bäumer, H.J. Freund, *Surf. Sci.* 399 (1998) 190.
- [79] J.B. Giorgi, T. Schroeder, M. Bäumer, H.J. Freund, *Surf. Sci.* 498 (2001) L71.
- [80] Y.X. Jiang, S.G. Sun, N. Dung, *Chem. Phys. Lett.* 344 (2001) 463.
- [81] G.Q. Lu, S.G. Sun, L.R. Cai, S.P. Chen, Z.W. Tian, *Langmuir* 16 (2000) 778.
- [82] S. Zou, M.J. Weaver, *Anal. Chem.* 70 (1998) 2387.
- [83] F. Maroun, F. Ozanam, O.M. Magnussen, R.J. Behm, *Science* 243 (2001) 1811.
- [84] K. Yoshimi, M.B. Song, M. Ito, *Surf. Sci.* 368 (1996) 389.
- [85] R.L. Borup, D.E. Sauer, E.M. Stuve, *Surf. Sci.* 374 (1997) 142.
- [86] X.Y. Zhu, J.M. White, M. Wolf, E. Hasselbrink, G. Ertl, *J. Phys. Chem.* 95 (1991) 8393.
- [87] J. Clavilier, R. Albalat, R. Gomez, J.M. Orts, J.M. Feliu, *J. Electroanal. Chem.* 360 (1993) 325.

- [88] N.P. Lebedeva, M.T.M. Koper, E. Herrero, J.M. Feliu, R.A. van Santen, *J. Electroanal. Chem.* 487 (2000) 37.
- [89] N.P. Lebedeva, J.M. Feliu, M.T.M. Koper, R.A. Van Santen, *J. Electroanal. Chem.* 524–525 (2002) 242.
- [90] N.P. Lebedeva, A. Rodes, J.M. Feliu, M.T.M. Koper, R.A. van Santen, *Phys. Chem. B* 106 (2002) 9803.
- [91] W. Akemann, A. Friedrich, U. Stimming, *J. Chem. Phys.* 113 (2000) 6864.
- [92] D.K. Lambert, *J. Chem. Phys.* 89 (1988) 3847.
- [93] A.B. Anderson, *J. Electroanal. Chem.* 280 (1990) 37.
- [94] S. Gilman, *J. Phys. Chem.* 68 (1964) 70.